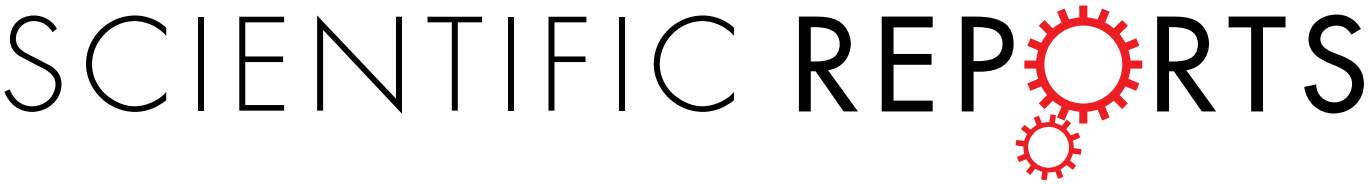

OPEN

Preferential Accumulation of Phospholipid-PEG and Cholesterol-PEG Decorated Gold Nanorods into Human Skin Layers and Their Photothermal-Based Antibacterial Activity

Received: 14 November 2018
Accepted: 21 March 2019
Published online: 08 April 2019

Nouf N. Mahmoud[1], Ala A. Alhusban[1], Jamila Isabilla Ali[1], Amal G. Al-Bakri[2], Rania Hamed[1] & Enam A. Khalil[2]

Herein, a library of gold nanorods (GNR) decorated with polyethylene glycol-thiol (PEG-SH) containing different functionalities were synthesized and characterized by optical absorption spectroscopy, zeta potential, dynamic light scattering (DLS), transmission electron microscope (TEM) and proton nuclear magnetic resonance (^{1}H-NMR). The colloidal stability of GNR when exposed to skin, and their preferential accumulation into excised human skin layers were investigated. Confocal laser scanning microscopy, transmission electron microscope (TEM) and inductively coupled plasma-optical emission spectroscopy (ICP-OES) were utilized to track the penetration of GNR into different skin layers. The results demonstrated that cholesterol-PEG coated GNR were preferentially loaded up in the upper layers of skin (stratum corneum), while phospholipid-PEG coated counterparts were drastically deposited in skin dermis. Neutral methoxy-PEG-coated GNR were distributed in both SC and dermis skin layers, while charged GNR (anionic-carboxylic acid-PEG-GNR and cationic-amine-PEG-GNR) revealed a minimal accumulation into skin. DSPE-PEG-GNR and Chol-PEG-GNR demonstrated antibacterial activities against *Staphylococcus aureus* (*S aureus*) at MIC values of 0.011 nM and 0.75 nM, respectively. Photothermal treatment for *S. aureus* at sub-MIC concentrations resulted in a significant bactericidal effect when using Chol-PEG-GNR but not DSPE-PEG-GNR. Gold-based nanoscale systems have great value as a promising platform for skin diseases therapy.

Skin is considered as the ideal site for non-invasive skin therapeutic platforms[1,2]. Stratum corneum (SC) consists of proteins and lipid matrix and limits the penetration of the topically applied drugs[3–5]. Chemical and physical penetration enhancers are commonly used to modulate the skin morphology at the molecular level[6,7]. Furthermore, dermal and transdermal drug delivery nanocarriers, such as polymers, liposomes, lipids and inorganic nanoparticles, can retard drugs' degradation, prolong their release, and enhance their solubility[8–11].

Among nano-systems, gold nanoparticles (GNP) and in particular, gold nanorods (GNR) have important applications in nanomedicine such as imaging, sensing, bio-tracking and photothermal therapy owing to their optical properties[12–15]. GNP of different shapes, sizes and surface functionalities were employed to probe the skin-nano interface[16]. For example, Sonavane *et al.* have demonstrated that the small-sized GNP penetrated into skin dermis[17], whereas Fernandes *et al.* revealed that GNP with rod-like shape have better penetration through skin compared to spherical counterparts[18]. Besides, negatively-charged skin components have repelled anionic nanoparticles, while higher affinity to SC has been reported using cationic nanoparticles[19]. Moreover, the surface

[1]Department of Pharmacy, Faculty of Pharmacy, Al-Zaytoonah University of Jordan, Amman, 11733, Jordan. [2]Department of Pharmaceutics & Pharmaceutical Technology, School of Pharmacy, The University of Jordan, Amman, 11942, Jordan. Correspondence and requests for materials should be addressed to N.N.M. (email: nouf.mahmoud@zuj.edu.jo)

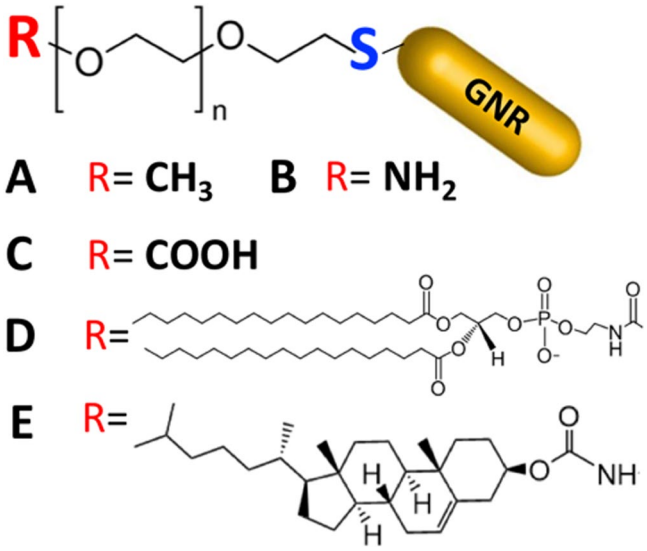

Figure 1. Illustration of different ligands containing PEG-SH used to functionalize the surface of GNR. (**A**) Methyl; (**B**) Amine; (**C**) Carboxylic acid; (**D**) Phospholipid (DSPE); and (**E**) Cholesterol.

modification of nanoparticles, such as proteins, lipids and oleic acids has increased the permeability and accumulation of nanoparticles into different skin compartments[18,20–23].

Phospholipids, the main component of the cell membrane, have been used as a biocompatible surface coating agent for many nanoparticles such as graphene, silica, inorganic nanoparticles and quantum dots[24–27]. Lipid-coated nanomaterials have great potentials for biomedical applications. For example, clusters of phospholipid-coated GNP and lipid-coated GNP have been used to enhance the theranostic effects, cellular uptake, drug delivery and cancer therapy of GNP[28–32].

Accumulation of nanomaterials at specific skin sites has a great impact on dermal drug delivery and tracking, in addition to their applications in diagnosis and skin diseases therapy[33]. In our earlier work, hydrophobic GNR coated with polystyrene-thiol were designed to be preferentially accumulated into human skin hair follicles, with minimal dermal distribution, as a promising platform for photothermal treatment of acne[34]. However, the interaction of phospholipid and cholesterol-modified-GNR with human skin and their accumulation potentials into skin layers have not been investigated fully in the literature.

The unique photothermal properties of GNR make them attractive anticancer and antibacterial candidates. GNR can convert the absorbed light into intense localized heat that could be effective for cancer and bacterial photothermal ablation[15]. Recently, the photo-thermolysis activity of GNR of hydrophilic or hydrophobic surface properties was evaluated against common skin bacteria such as *Propionibacterium acnes* and *Staphylococcus aureus* (*S. aureus*)[35]. In addition, photothermal ablation was reported for GNR conjugated to antibodies against *Pseudomonas aeruginosa*[36].

Taking into consideration the unique advantages of GNR as a "nano-model", their superiority in synthesis, colloidal stability, drug delivery and therapy, GNR decorated with PEG-thiol containing different functionalities were synthesized in this study, and their colloidal stability upon human skin contact was investigated. Employing confocal laser scanning microscopy, transmission electron microscopy (TEM) and inductively coupled plasma-optical emission spectroscopy (ICP-OES), the skin penetration and preferential accumulation of GNR decorated with phospholipid or cholesterol conjugated to PEG-thiol (SH) were probed and compared to that of GNR decorated with methoxy (m)-PEG or charged PEG moieties (carboxylic acid or amine groups). The effect of particle size and vehicle on the accumulation of GNR into skin layers was evaluated. Moreover, the antibacterial and photothermal-based antibacterial activities of DSPE-PEG-GNR and Chol-PEG-GNR were evaluated against *S. aureus*, a common skin pathogen.

Results and Discussion

Synthesis and characterization of GNR of different particle sizes and coated with PEG-SH-containing different functionalities. CTAB-assisted synthesis protocol was used to prepare GNR having aspect ratio (length/width; AR) of ~4 and ~2. This particular shape of GNP was selected owing to their uncommon optical characteristics, superior photothermal and antibacterial activities, and their potential accumulation into skin layers[13,15,18,35,37,38].

Due to the cellular toxicity of CTAB molecules[39], CTAB bilayers of GNR were replaced by ligand exchange using thiol-containing polyethylene glycol (PEG-SH). PEG-SH was utilized in this study as a binding ligand on GNR to facilitate the deposition of other functional moieties on the GNR surface *via* Au—S bonding (Fig. 1). PEG-SH is mostly used in ligand exchange reactions with GNR due to its high affinity to gold, well-known biocompatibility, and its key role in enhancing the GNR colloidal stability and disperse-ability in aqueous media[40–42]. Neutral m-PEG-coated GNR, anionic-COOH-PEG-coated GNR, cationic-NH_2-PEG-coated GNR, phospholipid

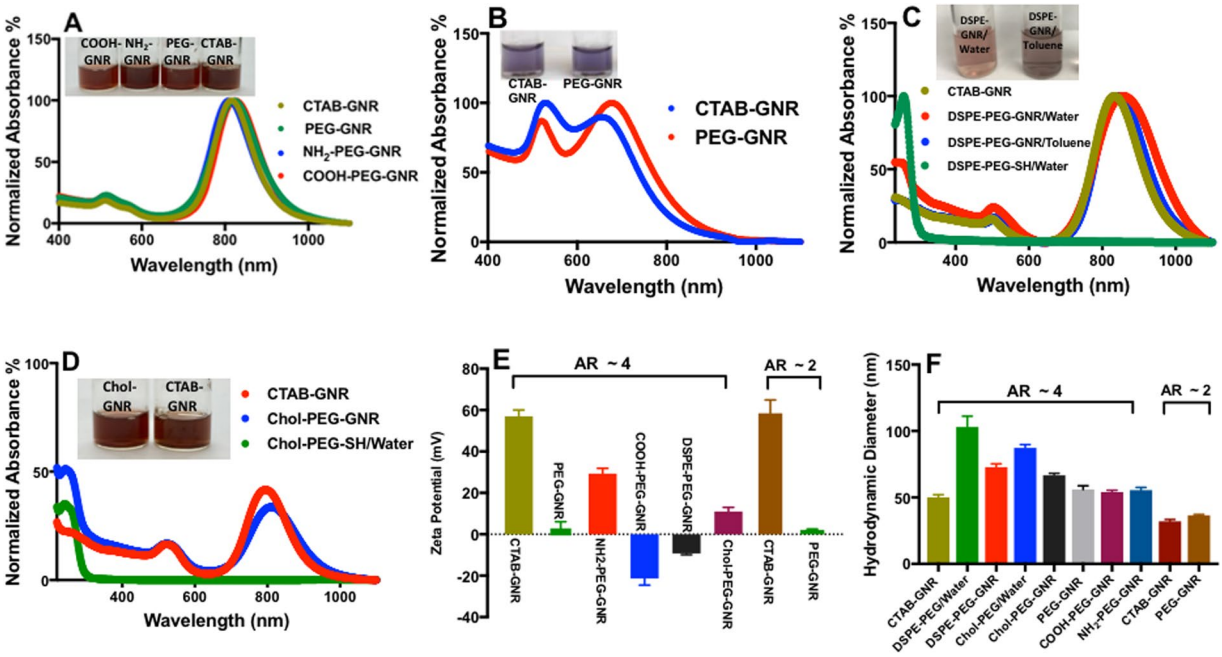

Figure 2. Characterization of GNR of different particle sizes and surface functionalities. (**A**) Optical absorption spectra and suspension photos of CTAB-GNR, m-PEG-GNR, NH_2-PEG-GNR and COOH-PEG-GNR (AR ~ 4). (**B**) Optical absorption spectra and suspension photos of CTAB-GNR and PEG-GNR (AR ~ 2). (**C**) Optical absorption spectra and suspension photos of CTAB-GNR, DSPE-PEG-GNR/water, DSPE-PEG-GNR/toluene and DSPE-PEG-SH/water. (**D**) Optical absorption spectra and suspension photos of CTAB-GNR, Chol-PEG-GNR and Chol-PEG-SH/water. (**E**) Zeta potentials of GNR of different particle sizes and surface functionalities (**F**) Hydrodynamic diameter of GNR of different particle sizes and surface functionalities measured by DLS (nm). Data in E and F are presented as mean ± SD (n = 3). AR: aspect ratio.

(DSPE)-PEG coated-GNR (suspended in water or toluene) and Chol-PEG-coated GNR suspensions were successfully synthesized and characterized by different microscopy and analytical instrumentation techniques. The optical absorption spectra of CTAB-GNR (AR ~ 4) demonstrated two typical plasmon peaks, at 520 nm and 830 nm, respectively (Fig. 2A), while CTAB-GNR (AR ~ 2) showed the plasmon peaks at 520 nm and 640 nm, respectively (Fig. 2B).

Upon surface modifications with PEG-SH of different functionalities, no tailing or broadening was observed in the optical spectra, indicating excellent stability of the synthesized colloids. However, a slight shift of the longitudinal peaks of the functionalized GNR was identified related to the refractive index of the coating moieties or the suspending solvents (in case of toluene) (Fig. 2A–D). The zeta potential of CTAB-GNR and the modified nanorods confirmed their successful functionalization with different PEG-SH containing ligands. CTAB-GNR of AR ~ 4 and ~2 demonstrated positive zeta potentials (+57 and +58 mV, respectively, Fig. 2E), whereas m-PEG-GNR of AR ~ 4 and ~2 showed neutral surface charges (+2.3 and +1.8 mV, respectively, Fig. 2E). The zeta potential values were high for both NH_2-PEG-GNR and COOH-PEG-GNR (+29.0 and −21.0, respectively, Fig. 2E). DSPE-PEG-GNR and Chol-PEG-GNR suspended in water demonstrated relatively low zeta potential values (−10.0 and +9.3, respectively; Fig. 2E). The average hydrodynamic diameter of CTAB-GNR of AR ~4 using DLS was ~52.0 nm, and it became ~69.7 nm and ~62.8 nm upon functionalization with DSPE-PEG-SH and Chol-PEG-SH, respectively. These shifts in hydrodynamic diameters suggest the formation of phospholipid-PEG and Chol-PEG layers covalently linked to GNR surface *via* thiol moieties (Fig. 2F). Besides, the hydrodynamic diameters for other modified GNR of AR ~ 4 and ~2 demonstrated slight increase in particles size upon surface modifications (Fig. 2F). The nanoparticles' shape and size and the absence of GNR aggregates upon functionalization were also verified by TEM. TEM imaging of PEGylated GNR of AR ~ 4 demonstrated average diameters of 47.1 nm and 12.7 nm for length and width, respectively and average AR of ~3.7 (Fig. 3A), while m-PEG-GNR of AR ~ 2 showed average diameters of 33.1 nm and 15.2 nm for length and width, respectively and average AR of ~2.1 (Fig. 3B). Further, TEM images of DSPE-PEG-GNR, Chol-PEG-GNR and other modified GNR of AR ~ 4 demonstrated well-dispersed rod-shaped nanoparticles having similar particle sizes without significant aggregation (Fig. 3C–F).

The displacement of CTAB bilayer by DSPE-PEG-SH or Chol-PEG-SH was monitored and confirmed by ^{1}H-NMR. The ^{1}H-NMR chemical shifts of DSPE-PEG-SH and its corresponding DSPE-PEG-GNR, and that of Chol-PEG-SH and its corresponding Chol-PEG-GNR are similar (the assigned intense PEG peak, hydrocarbon peak and other peaks, Figures S1A,B and S2A,B, Supplementary Information). However, some 1H-NMR peaks were slightly broadened or shifted upon conjugation with GNR, in which the thiolated ligand forms Au—S with gold atoms. Monitoring the conjugation of thiolated molecules to GNP by ^{1}H-NMR was described previously in

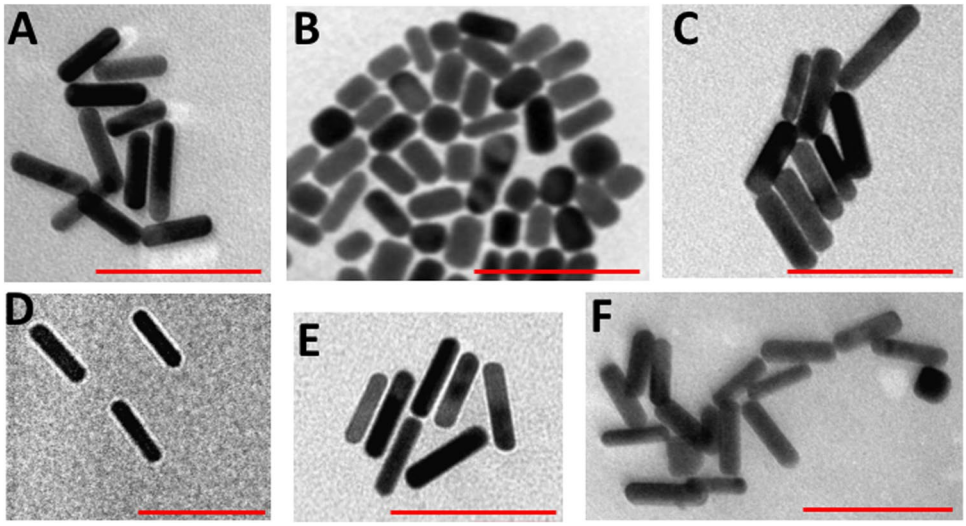

Figure 3. Transmission electron microscope images of GNR of different particle sizes and surface functionalities. (**A**) m-PEG-GNR (AR ~ 4), (**B**) m-PEG-GNR (AR ~ 2), (**C**) COOH-PEG-GNR (AR ~ 4), (**D**) DSPE-PEG-GNR (AR ~ 4), (**E**) Chol-PEG-GNR (AR ~ 4). (**F**) NH_2-PEG-GNR (AR ~ 4). Scale: 100 nm.

the literature, where the ^{1}H-NMR spectra demonstrated complicated changes upon binding of thiol terminated ligands to the surface of GNP. This was explained by the vicinity of the molecules to the GNP surfaces[43,44].

Understanding the interaction of DSPE-PEG-SH or Chol-PEG-SH with CTAB-GNR is provided by comparing the ^{1}H-NMR spectra of the thiolated ligands and the modified GNR with the ^{1}H-NMR spectrum of CTAB-GNR (Figures S1 and S2, Supplementary Information). While many of the ^{1}H-NMR peaks of CTAB overlapped with that of DSPE or cholesterol spectra, the γ-methyl peak for CTAB attached to GNR (δ ~ 3.39 ppm) is clearly distinct[45]. Upon addition of DSPE-PEG-SH or Chol-PEG-SH, a dramatic reduction of the intense γ-methyl peak of the CTAB-coated GNR at ~3.39 ppm, and a complete elimination of the small peak related to the protons attached to C1 of CTAB were observed in the spectra of DSPE-PEG-GNR and Chol-PEG-GNR. Also, a new sharp proton peak represents the repeated units of PEG at ~3.68 ppm appeared. An extra small peak at ~1.7 ppm of the ^{1}H-NMR spectrum of CTAB-GNR is most likely due to a trace impurity[46].

It is worth mentioning that CTAB-GNR suspension was centrifuged twice before addition of the thiolated ligands, and one more time after an overnight mixing with the thiolated ligands in order to remove free CTAB from the suspensions. Furthermore, the ligands were added to CTAB-GNR in excess to facilitate the CTAB displacement process. The above ^{1}H-NMR results clearly demonstrate the successful displacement of nanorods-bound CTAB by the addition of DSPE-PEG-SH or Chol-PEG-SH. Similar results were demonstrated by Orendorff *et al.* using ^{1}H-NMR to follow the interaction of a phospholipid with the CTAB-GNR composite[45].

Colloidal stability of GNR coated with PEG-SH-containing different functionalities upon human skin contact. The colloidal stability of many nanoparticles when interacting with skin is ignored in the majority of skin permeation and diffusion studies, which might be responsible for the observed conflicting results. Accordingly, prior to investigating the penetration of GNR into skin layers, their colloidal stability upon exposure to skin surface was examined. Previously, we have reported an enhanced aggregation of functionalized GNR with electrostatic-attracted cationic groups relative to their anionic PEGylated counterparts due to protein adsorption upon contact with human skin[42]. Herein, the colloidal stability of the surface modified GNR was evaluated upon exposure to human skin by inspecting their colloidal color changes, and by measuring their optical absorption spectra at zero time and after 24 hr of skin contact. Interestingly, all GNR of different functionalities containing PEG-SH demonstrated no color change and exhibited typical plasmon peaks with slight broadening of the longitudinal peaks after 24 hr of skin exposure (Fig. 4A–F). The colloidal stability of GNR suspensions was inspected also by recording the nanoparticles' hydrodynamic size and zeta potential before and after skin exposure (Table 1). No significant differences in the particle sizes or zeta potentials were reported after 24 hr, which confirm the excellent colloidal stability of the nanorods upon human skin exposure.

The stabilization effect of PEG on GNR is well-demonstrated in the literature, where the presence of PEG layer stabilizes the nanoparticles and retards the adsorption of proteins onto their surfaces by steric repulsion[47]. Further, the presence of PEG-SH, especially for DSPE and cholesterol moieties, enhances their water disperse-ability[48]. It is important to mention that DSPE-PEG-SH and Chol-PEG-SH were added to GNR suspensions in excess, in order to provide a full coverage of GNR with thiolated ligands and to prevent their aggregation.

The penetration and accumulation of GNR of different particle sizes and different surface functionalities into human skin layers. In order to preserve human skin structural integrity and to minimize artifacts and co-factors, the experimental human skin was used within a very short time of excision (5 days).

The interaction of CTAB-GNR with skin was not investigated in this study owing to their well-known significant cytotoxicity and poor colloidal stability[49].

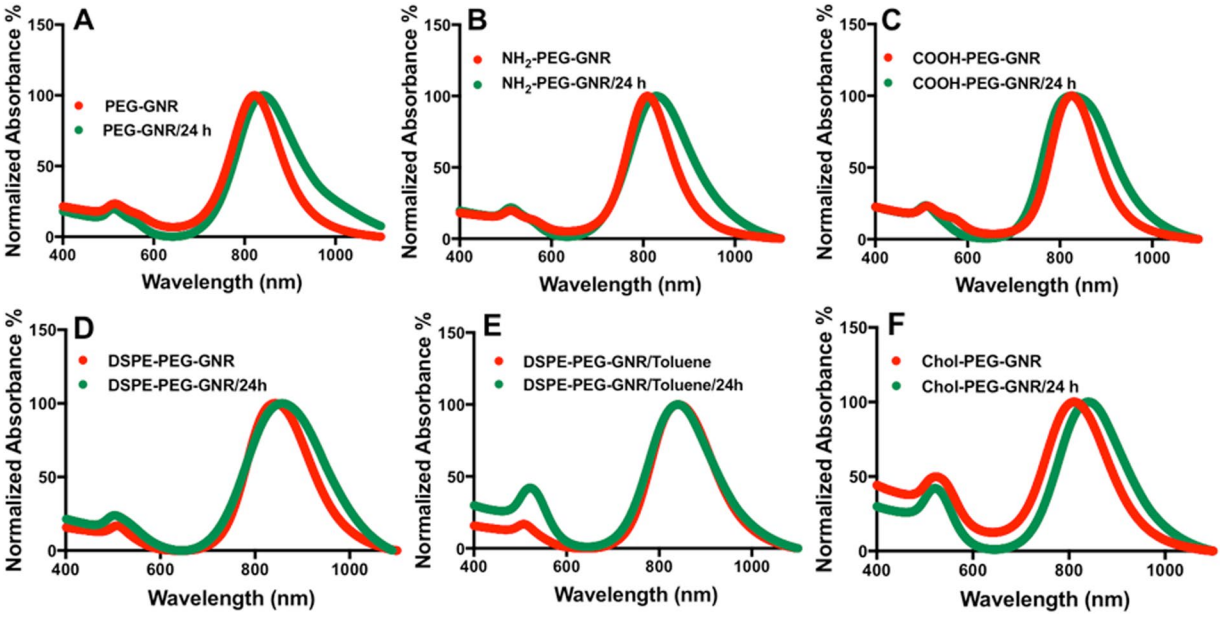

Figure 4. Optical absorption spectra of GNR of different surface functionalities (AR ~ 4) before (red lines) and after 24 hr of skin contact (green lines). (**A**) m-PEG-GNR, (**B**) NH_2-PEG-GNR, (**C**) COOH-PEG-GNR, (**D**) DSPE-PEG-GNR. (**E**) Chol-PEG-GNR. All spectra reveal no significant tailing or broadening of the plasmon peaks that indicates excellent colloidal stability of GNR suspensions upon skin exposure.

GNR	Hydrodynamic size (nm)		Surface charge (mV)	
	Before skin contact	*After skin contact*	*Before skin contact*	*After skin contact*
m-PEG-GNR	51.2 ± 2.1	53.5 ± 2.6	+2.3 ± 0.9	+0.9 ± 0.09
NH_2-PEG-GNR	50.2 ± 3.2	54.1 ± 3.3	+30.0 ± 1.0	+20.3 ± 0.8
COOH-PEG-GNR	52.4 ± 0.9	55.1 ± 2.5	−22.2 ± 0.5	−26.8 ± 1.1
DSPE-PEG-GNR	67.8 ± 1.9	74.9 ± 1.7	−13.6 ± 0.7	−11.5 ± 0.8
Chol-PEG-GNR	65.6 ± 2.1	69.2 ± 2.1	+11.2 ± 2.3	+9.3 ± 2.6

Table 1. Hydrodynamic sizes measured by DLS, and effective surface charges of GNR of different surface functionalities before and after human skin contact for 24 hr. Data are given as mean ± SD (n = 3).

Human skin is composed of SC (made of proteins and lipids), epidermis and a more hydrophilic lower layer called dermis[50]. The preferential accumulation of GNR having the same particle size and different surface functionalities and zeta potential values into skin layers was evaluated quantitatively by measuring the amount of gold deposited into skin SC or dermis. Figure 5 illustrates the percentage of the initial gold dose of GNR that accumulated in SC and dermis and that delivered trans-dermally into the acceptor media. Chol-PEG-GNR were significantly accumulated into the SC (~15.5%), compared to DSPE-PEG-GNR (~8.0%), m-PEG-GNR (~7.0%) or charged-GNR (NH_2-PEG-GNR or COOH-PEG-GNR) (<5%)(Fig. 5A). Interestingly, DSPE-PEG-GNR revealed high percentage of accumulation into skin dermis (~23.5%) compared to Chol-PEG-GNR (~8.5%) or neutral charged m-PEG-GNR (~11.0%) (Fig. 5B). However, charged-GNR with high zeta potential values (NH_2-PEG-GNR and COOH-PEG-GNR) demonstrated minimal accumulation percentages into skin dermis (Fig. 5B). For GNR that were delivered trans-dermally into the acceptor media, DSPE-PEG-GNR present the highest percentage of transdermal delivery (~2.0%), compared to other modified-GNR (Fig. 5C). PEGylated nanorods with a spheroid shape (AR of ~2) showed a significant accumulation into skin dermis compared to their counterparts having AR of ~4, while their accumulation into the SC was significantly less than that of nanorods with AR ~ 4. Both sizes of PEGylated nanorods revealed low concentrations in the acceptor media (Fig. 5D).

In order to probe the effect of the solvent on the penetration of GNR into skin, DSPE-PEG-GNR were suspended in water and in toluene. Although the penetration of DSPE-PEG-GNR-suspended in water into SC or dermis was slightly higher than that of DSPE-PEG-GNR-suspended in toluene, the difference was not statistically significant (Fig. 5A and B). In tune with other study, toluene does not have substantial enhancement effect on skin penetration, because toluene cannot extract ceramides, which are the main lipids constituents of SC[51].

Furthermore, the preferential accumulation of GNR into skin layers was evaluated by confocal laser scanning microscopy, due to the unique light scattering properties obtained by GNP[52]. The control skin sample showed a negligible fluorescence background (Fig. 6A), while an appreciable fluorescence was perceived in the SC layers

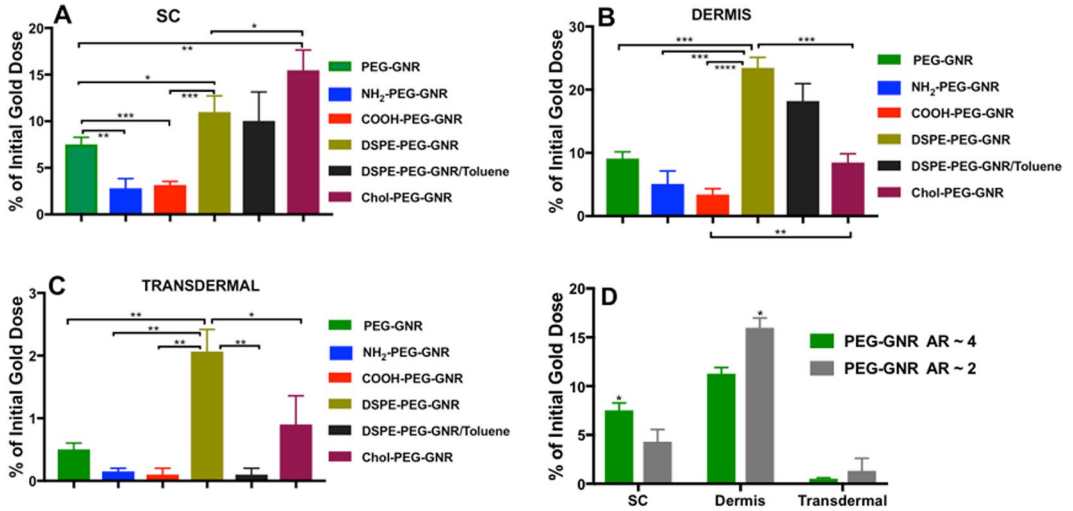

Figure 5. Percentages of GNR of different particle sizes and surface functionalities that accumulated into skin layers after 24 hr of incubation. (**A**) Percentages of GNR (AR ~ 4) accumulated into SC. (**B**) Percentages of GNR (AR ~ 4) accumulated into dermis. (**C**) Percentages of GNR (AR ~ 4) delivered transdermally into the acceptor media. (**D**) Percentages of PEG-GNR (AR ~ 4 *vs.* AR ~ 2) that accumulated into SC, dermis or delivered transdermally into the acceptor media. Data are presented as mean ± SD (n = 4). Unpaired t-test was used to assess the differences; *$p < 0.05$, **$p < 0.01$, ***$p < 0.001$ and ****$p < 0.0001$. AR: aspect ratio.

of skin incubated with Chol-PEG-GNR compared to DSPE-PEG-GNR (Fig. 6B,C,E,F). On contrast, enormous fluorescence was remarked in the dermis layer of skin treated with DSPE-PEG-GNR relative to Chol-PEG-GNR, which confirms the preferential accumulation of DSPE-PEG-GNR into skin dermis (Fig. 6G–I and D).

Figure S3, Supplementary Information, demonstrates the fluorescence of skin treated with m-PEG-GNR, COOH-PEG-GNR and NH_2-PEG-GNR. Moderate fluorescence intensities were noticed in SC and dermis of skin treated with m-PEG-GNR (Figure S3A,B, Supplementary Information). On the other hand, low fluorescence intensities were recorded for the upper layers of skin pre-treated with charged-PEGylated GNR (COOH-PEG-GNR and NH_2-PEG-GNR), which confirm the key role of the nanoparticles' surface chemistry in determining their preferential accumulation into different skin layers (Figure S3C–F, Supplementary Information).

The fluorescence intensity of the confocal fluorescence images was quantified and graphed in order to correlate their results with ICP-OES findings. The estimated fluorescence intensities of skin treated with GNR of different surface functionalities are in agreement with their quantities measured by ICP-OES; where Chol-PEG-GNR and DSPE-PEG-GNR showed the highest accumulation percentages in SC and dermis, respectively (Figure 4SA,B, Supplementary Information).

Moreover, the accumulation of GNR into the skin layers was visualized by TEM. DSPE-PEG-GNR are presented as black rod-shaped nanoparticles in the upper skin layers (Fig. 7A). In agreement with the previous results of ICP-OES and confocal fluorescence imaging, DSPE-PEG-GNR were highly deposited into the deep skin layers as small "aggregates" (Fig. 7B and C). The SC and dermis of control skin samples treated with milli-Q water demonstrated no characteristic dark rod-shaped nanoparticles (Fig. 7D and E, respectively). Figure 7F demonstrates a TEM image of GNR suspension that showed similarity between the particles' shape and size to those accumulated into skin.

Understanding and evaluating the penetration of topically applied nanomaterials into skin layers have been the focus of many recent studies. For examples, zinc oxide nanoparticles accumulated in the SC, although they demonstrated *in vitro* toxicity[53,54]. Liquid colloidal systems such as nanoemulsions are enhancing the dermal drug delivery by disruption of SC lipid, however they have poor stability and could cause skin irritation[55,56]. Furthermore, solid lipid nanoparticles demonstrated a shape deformation after application to skin and enhancing the dermal penetration of the loaded drugs[57]. However, their low drug loading capacity and poor stability limit their applications[58]. The penetration and preferential accumulation of the nanomaterials into skin layers were strongly correlated to their sizes and surface functionalities. For examples, Prow *et al*. found that PEGylated quantum dots were deposited into the epidermis of skin and not dermis compared to PEG-NH_2 or PEG-COOH which demonstrated no skin penetration at all[59]. Also, Zhang *et al*. have found that nanoparticles made of poly (d,l-lactic-co-glycolic acid) accumulated in the epidermis rather than the dermis, and their skin permeation was highly correlated to the particle size[60].

The effect of phospholipids on the uptake of nanoparticles into cells or tissues was evaluated in the literature using liposomes as a model. Liposomes can enhance the transdermal drug delivery, although their penetration through SC is limited[61]. Liposomes have some disadvantages such as instability, low solubility, rapid elimination from the blood and leakage of the loaded drugs[61]. Compared to many other nano-systems, GNP are superior in synthesis and chemical stability, and their surfaces can be easily modified with different ligands at a density of 100-fold higher than that of liposomes[62]. In addition, GNP can be easily quantified and tracked within

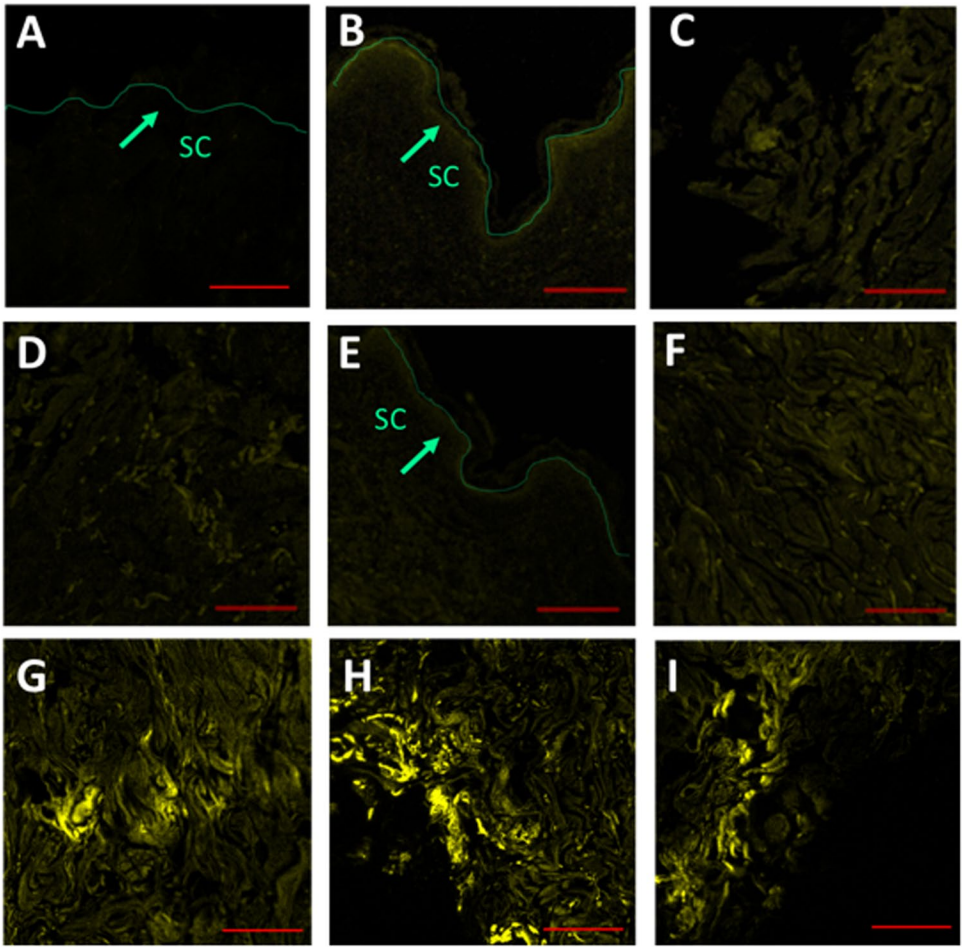

Figure 6. Confocal laser scanning microscopy images of skin samples pre-treated with DSPE-PEG-GNR or Chol-PEG-GNR. (**A**) SC of skin sample pre-treated with milli-Q water as a control. (**B**) SC of skin sample pre-treated with Chol-PEG-GNR. (**C**) High magnification of SC of skin sample pre-treated with Chol-PEG-GNR. (**D**) Dermis layer of skin sample pre-treated with Chol-PEG-GNR. (**E**) SC of skin sample pre-treated with DSPE-PEG-GNR. (**F**) High magnification of SC of skin sample pre-treated with DSPE-PEG-GNR. (**G**–**I**) Dermis layers of skin samples pre-treated with DSPE-PEG-GNR. Scales: **A**, **B** and **E** = 200 μm, **C**, **D**, **F**–**I** = 100 μm.

the biological systems owing to their high electron density[13,14]. Moreover, their biomedical applications extend beyond drug delivery vehicle to diagnosis and sensing applications, in addition to photothermal therapy.

Generally, the nano-bio interface is highly impacted by chemical and physical characteristics of the nano-system in addition to the properties of the biological barrier. In previous studies, it was demonstrated that phospholipids can penetrate and disturb the structure of SC lipids due to lipid mixing effect between phospholipids and SC lipids using liposomes as a model[63,64]. Kirjavainen *et al*., concluded that phospholipids acted as enhancers and increased the distribution of drugs into the SC by increasing the fluidity of SC lipids[65]. Based on the current results, we suppose that cholesterol and phospholipid enhanced the penetration of GNR through the upper skin layers due to their proposed modulation effect on the lipid contents of SC which consists mainly of ceramides, fatty acids, cholesterol and cholesteryl esters[3,4,7]. Also, we propose that the hydrophilic nature of the dermis probably retarded any further penetration of Chol-PEG-GNR into the deep skin layers compared to DSPE-PEG-GNR. These results agreed with our previous findings, where the penetration of hydrophobic polystyrene-thiol coated-GNR into skin dermis was limited by the hydrophilic nature of the dermis[34]. The preferential drastic accumulation of DSPE-PEG-GNR into deep skin layers was probably owing to their amphiphilic properties, which enhanced their distribution into the deep hydrophilic skin layers through SC. Similarly, Iannuccelli *et al*., have found that coating silica nanoparticles with lipids has drastically increased their penetration into human SC compared to the hydrophilic counterparts[66]. In addition to the drastic impact of phospholipids in cellular/tissues uptake, the colloidal stability was enhanced for many nanoparticles modified with a phospholipid bilayer[27,67].

Neutral charged PEGylated GNR were distributed into upper and lower skin layers which is most likely due to their hydrophilic-hydrophobic properties and their penetration enhancing activity[68]. However, the charged PEGylated nanorods with high zeta potential values demonstrated the lowest percentage of accumulation into skin layers. These results are in concordance with previous studies using charged non-PEGylated nanoparticles[34,66].

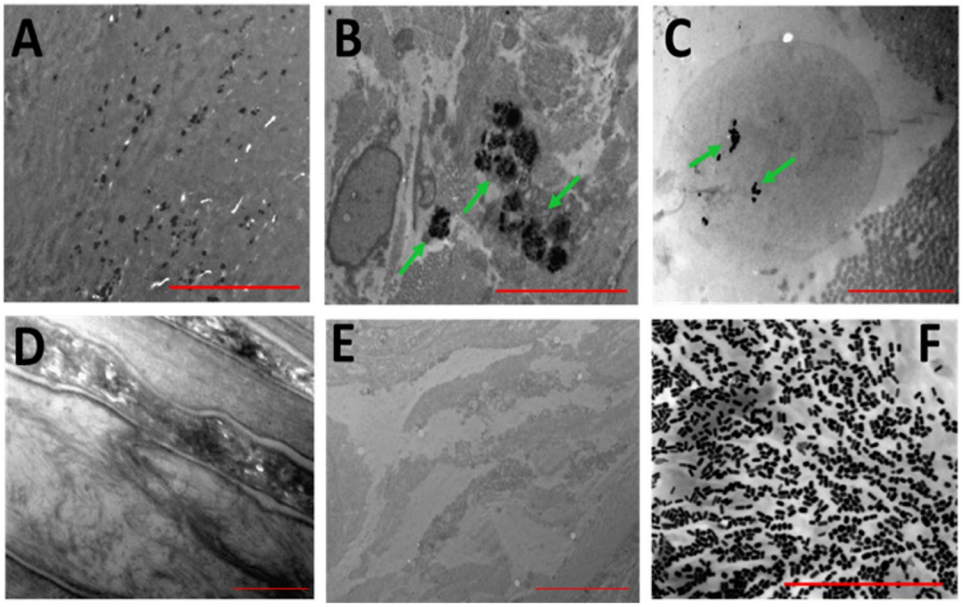

Figure 7. Transmission electron microscope images presenting the distribution of DSPE-PEG-GNR into skin layers. (**A**) SC showing the rod-shape of the penetrated GNR. (**B**,**C**) Clusters of GNR at skin dermis. (**D**,**E**) SC and dermis of skin treated with milli-Q water, respectively (as control). (**F**) Transmission electron microscope of GNR suspension to compare their shape and particle size to those accumulated into skin. Scales: **A**, **C**, **D** and F = 2 μm; (**B**,**E**) = 5 μm.

GNR	MIC (nM)*	Reduction of viable count (%)	Log reduction
DSPE-PEG-GNR	0.011	99.99 ± 0.0025	4.0
Chol-PEG-GNR	0.75	99.56 ± 0.05	2.3

Table 2. Minimum inhibitory concentration (MIC) values of DSPE-PEG-GNR and Chol-PEG-GNR against *S. aureus* and the percentage and log reduction of *S. aureus* viable count at the MIC values. Data are presented as mean ± SD (n = 3). *SD for MIC values are zero.

The accumulation potential of m-PEG-GNR of different aspect ratios was evaluated in this study to understand the impact of particle size on the interaction of GNR with human skin layers. Interestingly, PEGylated nanorods with AR of ~2 (spheroids) demonstrated high accumulation percentage into skin dermis compared to the PEGylated nanorods with AR of ~4. Several studies reported that as the gold nanospheres' size decreases, their accumulation into skin are enhanced[17,69]. However, reports evaluating interaction of different sizes of GNR with skin are lacking in the literature. Fernandes *et al*. have found that the total percentage of GNR in skin was higher than that of gold nanospheres, however, no data regarding the percentage in each skin layer was provided[18].

The results of the transdermal delivery of GNR into the acceptor media of Franz diffusion cells (FDCs) revealed that DSPE-PEG-GNR could be successfully employed for transdermal drug delivery *via* skin, although the percentage of GNR delivered transdermally was very low (~2.0%).

The overall results demonstrated that preferential accumulation of GNR into human skin layers was strongly associated with their surface functionality.

Antibacterial and Photothermal-based antibacterial activities of DSPE-PEG-GNR and Chol-PEG-GNR against *S. aureus*. The photothermal therapy of GNR is a cornerstone in their nanomedicine and biomedical applications[13]. As DSPE-PEG-GNR and Chol-PEG-GNR have demonstrated the highest percentages of accumulation into skin, we have investigated the antibacterial activity and photothermal-based antibacterial ablation effect of DSPE-PEG-GNR and Chol-PEG-GNR against *S. aureus*, the leading cause of soft tissues and skin infections[70]. The antibacterial effect of GNR was explored by estimating the minimum inhibitory concentrations (MIC) and percentage reduction of *S. aureus* viable count at the MIC values[71,72]. MIC is the lowest concentration of the agent that prevents the visible growth of a pathogen[71].

Table 2 represents the MIC values of DSPE-PEG-GNR and Chol-PEG-GNR against *S. aureus*. Interestingly, phospholipid-coated GNR resulted in 4-log reduction (99.99%) in bacterial viable count at its MIC value (0.011 nM). However, cholesterol-coated GNR showed only 2-log reduction (99%) in bacterial viable count at its MIC value (0.75 nM). The coating materials (DSPE-PEG-SH and Chol-PEG-SH) demonstrated no antibacterial activity against *S. aureus*.

	Reduction of viable count (%)	Log reduction
DSPE-PEG-GNR		
0.004 nM	91.0 ± 0.20	1.0
0.004 nM + Laser	98.0 ± 0.07	1.7
0.002 nM	93.8 ± 0.70	1.2
0.002 nM + Laser	99.0 ± 0.70	2.0
Laser	93.5 ± 2.2	1.2
Chol-PEG-GNR		
0.125 nM	93.0 ± 4.2	1.1
0.125 nM + Laser	99.99 ± 0.003	4.0
0.06 nM	86.5 ± 2.1	0.87
0.06 nM + Laser	99.6 ± 0.14	2.4
Laser	93.5 ± 2.2	1.2

Table 3. Percentage and log reduction of *S. aureus* viable count after DSPE-PEG-GNR and Chol-PEG-GNR treatments with and without laser at sub-MIC concentrations. Data are presented as mean ± SD (n = 3).

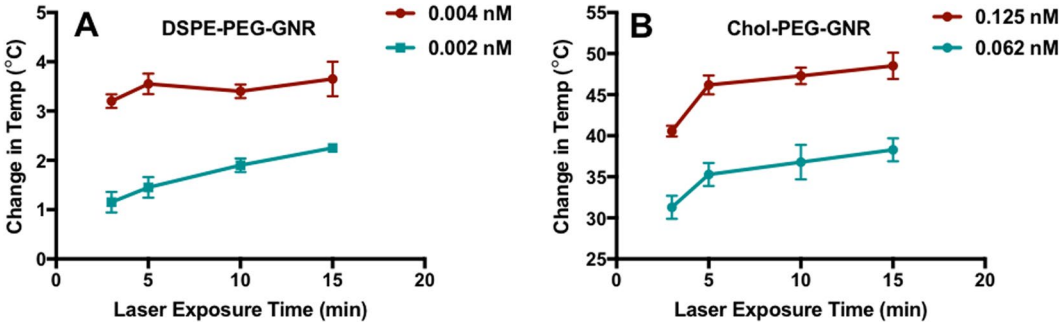

Figure 8. Temperature changes induced by NIR laser excitation of GNR suspensions over 15 min. (**A**) Temperature change of DSPE-PEG-GNR suspension at sub-MIC concentrations upon laser exposure. (**B**) Temperature change of Chol-PEG-GNR suspension at sub-MIC concentrations upon laser exposure. The initial temperature was 19.7 ± 0.4 °C. Data are presented as mean ± SD (n = 3).

This is the first study to report the antibacterial activity of lipid-coated GNR against Gram positive bacteria such as *S. aureus*. Previously, phospholipid stabilized silver nanoparticles demonstrated a weak bactericidal activity against *S. aureus* (70%)[73].

Furthermore, the photothermal ablation effect of phospholipid and cholesterol-modified GNR against *S. aureus* was investigated in this study upon laser beam treatment over concentrations below the MIC values. The laser excitation time was set to 15 min since aggregation of the nanorods was observed after more than 15 min of laser exposure[35]. The changes in GNR suspension temperature upon exposure to the laser beam was recorded over time and the photothermal-based antibacterial activity was evaluated using the standard plate viable count method[72]. For DSPE-PEG-GNR, laser excitation resulted in no additional reduction in *S. aureus* viable count over concentrations below the MIC value (0.004 and 0.002 nM) compared to the combined effect of the controls (GNR or laser alone) (Table 3). A slight increase in DSPE-PEG-GNR suspensions' temperature upon excitation with the laser was reported over 15 min relative to the initial temperature (Fig. 8A).

On the other hand, Chol-PEG-GNR demonstrated an extra 2-log reduction in *S. aureus* viable count at concentration of 0.125 nM (sub-MIC) compared to the combined effect of the controls (GNR or laser alone) (Table 3). A significant increase in Chol-PEG-GNR suspension's temperature over 15 min of laser exposure was recorded relative to the initial temperature (~65 *vs.* ~19.7 °C) (Fig. 8B). Chol-PEG-GNR at 0.06 nM (sub-MIC) did not result in any extra bactericidal activity compared to the combined effect of the controls although the temperature of the GNR suspension was increased by 35 °C over 15 min of laser exposure compared to the initial temperature (~46 *vs.* ~19.7 °C) (Fig. 8B).

The recorded localized heat obtained upon NIR excitation correlates well with the percentage of *S. aureus* viable count reduction which confirms the role of photothermal therapy in bacterial cells ablation. However, the photothermal antibacterial activity was not significant at the sub-MIC values of DSPE-PEG-GNR suspension, due to the low concentration of the photothermal-triggering species, the DSPE-PEG-GNR at these concentrations. The photothermal antibacterial activity of Chol-PEG-GNR at 0.06 nM resulted in no additional reduction of *S. aureus* viable count although the generated localized heat was increased by 35 °C at this concentration. This emphasizes the key role the surface functionality of GNR plays in delivering the nanorods into bacteria and consequently maximizing the photothermal effect. For effective photothermal therapy, the nanorods should be at

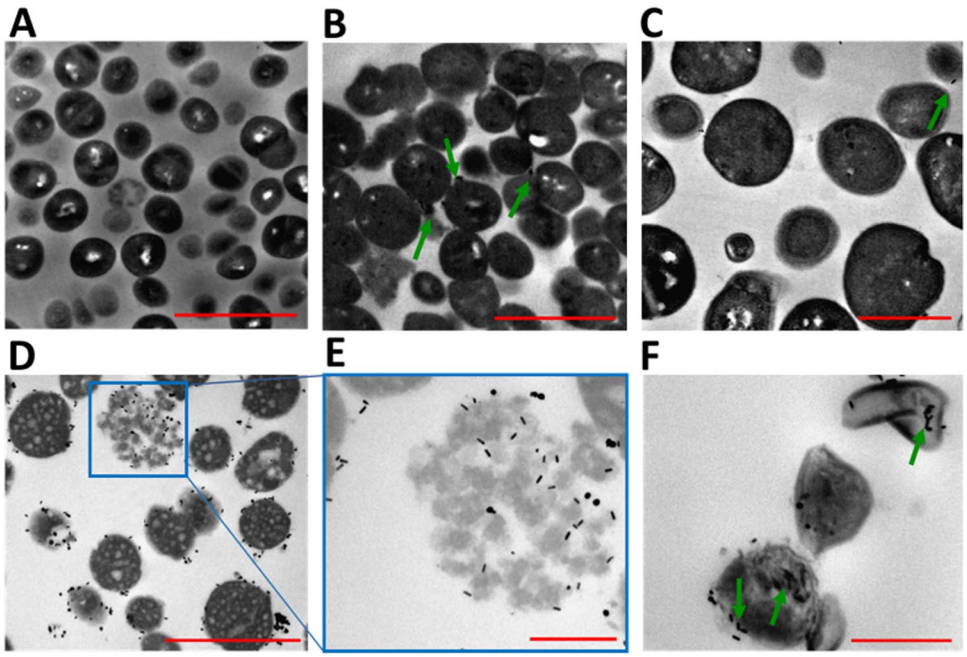

Figure 9. Transmission electron microscope images of *S. aureus* pre-treated with GNR. (**A**) Untreated *S. aureus* as control. (**B**,**C**) *S. aureus* treated with Chol-PEG-GNR. (**D**–**F**) *S. aureus* treated with DSPE-PEG-GNR. Arrows indicate the presence of GNR. Scales: (**A**,**B** and **D**): 2 μm, (**C**): 1 μm and (**E**,**F**): 0.5 μm.

least adsorbed onto the targeted cell surface, so the generated heat obtained upon NIR laser excitation can cause the required cell damage[15]. Accordingly, we suppose that the phospholipid utilized to modify the surface of GNR has enhanced the adsorption of the nanorods into the bacterial membrane and might facilitated their bacterial uptake and subsequently their bactericidal activity. That is why DSPE-PEG-GNR demonstrated very low MIC value compared to Chol-PEG-GNR (0.011 *vs*. 0.75 respectively; ~68 folds).

The antibacterial and photothermal-based antibacterial activities of m-PEG-GNR were investigated in our previous work. PEGylated GNR have MIC value of ~0.45 nM against *S. aureus* and demonstrated 4-log reduction in *S. aureus* viable count at concentration range of 0.06–0.25 nM upon treatment with NIR laser beam light[35,37].

The photo-thermolysis of bacteria employing GNR was described in the literature, however, the photothermal ablation activity of lipid-coated nanorods was not discussed before. Millenbaugh *et al*. reported that the laser-activated gold nanospheres conjugated with antibodies reduced *S. aureus* viability to 31%[74], which is a very weak effect in comparison to what is reported in the current study.

Imaging of *S. aureus* pre-treated with Chol-PEG-GNR or DSPE-PEG-GNR by TEM. The interaction of Chol-PEG-GNR or DSPE-PEG-GNR with *S. aureus* was further investigated using TEM imaging. Figure 9A represents a TEM image of untreated *S. aureus* as a control and indicates the intact shape of bacterial cells. Chol-PEG-GNR did not result in significant damage to *S. aureus* as presented in Fig. 9B,C. However, *S. aureus* pre-treated with DSPE-PEG-GNR demonstrated significant decrease in number and revealed notable bacterial uptake of the nanorods as presented in Fig. 9D–F. In addition, *S. aureus* showed significant disintegration and lysis upon treatment with DSPE-PEG-GNR as presented in Fig. 9D–F. The TEM images correlate well with the antibacterial activity of GNR, and clearly justified the potent bactericidal effect of DSPE-PEG-GNR, where phospholipid drastically enhanced the bacterial uptake and toxicity of GNR.

In conclusion, the preferential accumulation of GNR into skin layers was strongly associated with their surface chemical decoration. Phospholipids drastically enhanced GNR accumulation in skin dermis *via* SC, while cholesterol coated GNR were confined to the upper layers of SC with a minimum accumulation in the lower hydrophilic skin dermis. DSPE-PEG-GNR and Chol-PEG-GNR demonstrated reasonable antibacterial and photothermal-based bactericidal activities against *S. aureus*, the most common skin pathogen. Based on these findings, DSPE-PEG-GNR or Chol-PEG-GNR could be considered as a promising nano-therapy for skin diseases such as acne and skin infections.

Materials and Methods

Materials and instrumentations. Ascorbic acid (99%) chloroauric acid ($HAuCl_4.3H_2O$, 99.9%), methoxy-polyethylene glycol-thiol (m-PEG-SH, MW ~2000 g/mole), silver nitrate ($AgNO_3$, 99%), carboxylic acid PEG-thiol (COOH-PEG-SH, MW ~2000 g/mole), sodium borohydride ($NaBH_4$, 99%), amine PEG-thiol (NH_2-PEG-SH, MW ~2000 g/mole), cetyltrimethylammonium bromide (CTAB, 99%), gold standard for ICP (1000 PPM) and glutaraldehyde solution were obtained from Sigma-Aldrich Chemicals, USA. 1,2-distearoyl-sn-glycero-3-phosphoethanolamine-N-PEG-SH (DSPE-PEG-SH, MW~2000 g/mole) and cholesterol-PEG-SH

(MW~2000 g/mole) were obtained from Nanosoft Polymers, USA. 96 well-plates were purchased from Greiner bio- one, Germany. Nutrient agar, Mueller–Hinton broth, *S. aureus* ATCC 29213 were obtained from Oxoid, UK.

The following instruments were used in the study: Spectrophotometer (UV-1800, Shimadzu, Japan) was used for measuring the optical absorption spectra of GNR. Nicomp Nano Z3000 zeta potential/particle size analyzer (CA, USA). Versa 3D, FEI, Holland was used for TEM imaging. Hettich EBA 12 Centrifuge (Gemini BV, Netherland) was used for GNR centrifugation. Confocal laser scanning microscopy, LSM 780 (Carl Zeiss, Germany) was used for skin samples imaging. Optima 2000 DV (ICP-OES, PerkinElmer Corporation of USA) was used for gold analysis. All proton nuclear magnetic resonance (^{1}H-NMR) spectra were measured at 19.15 °C in Deuterated chloroform ($CDCl_3$) using Bruker AVANCE 300 MHz NMR instrumentation, Germany, operating at 300.13 MHz. Franz diffusion cells (FDCs), 1.0 cm^2 area were obtained from PermeGear Inc., USA. TEM grids (Formvar-coated) were obtained from Electron Microscopy Sciences, USA. Laser diode, Max power output ~9 W, 808 nm was purchased from OSTECH, Germany. A digital thermometer probe was purchased from FLIR Commercial Systems Inc., USA.

Methods. *Chemical synthesis of CTAB-coated GNR (CTAB-GNR) of aspect ratio (AR) ~4 and ~2.* CTAB-GNR were prepared using CTAB as a surfactant as described previously[34]. Briefly, $NaBH_4$ was added to a mixture of CTAB and gold solution to form seeds. For growth of GNR, $AgNO_3$ (1.3 mL, 0.01 M) was added to a solution of CTAB to acquire GNR with AR of ~4. After that, $HAuCl_4$ solution, ascorbic acid and the seeds were added to the growth solution and incubated at 27 °C overnight. GNR suspension was spun down twice by centrifugation at 12000 rpm for 15 min and re-suspended in milli-Q water. The previous procedure was repeated using 0.3 mL of $AgNO_3$ to obtain CTAB-GNR of AR ~ 2.

Surface modification of GNR with m-PEG-SH (PEG-GNR). A volume of 1.0 mL of aqueous solution of m-PEG-SH (15 mg/mL) was transferred to 10.0 mL of CTAB-coated GNR suspension and mixed overnight. The PEGylated GNR suspension was spun down twice by centrifugation at 10 000 rpm for 10 min and re-suspended in milli-Q water.

Surface modification of GNR with anionic COOH-PEG-SH (COOH-PEG-GNR). A volume of 1.0 mL of aqueous solution of COOH-PEG-SH (15 mg/mL) was transferred to 10.0 mL of CTAB-coated GNR suspension and mixed overnight. The coated GNR suspension was spun down twice by centrifugation at 10 000 rpm for 10 min and re-suspended in milli-Q water.

Surface modification of GNR with cationic NH_2-PEG-SH (NH_2-PEG-GNR). A volume of 1.0 mL of aqueous solution of NH_2-PEG-SH (15 mg/mL) was transferred to 10.0 mL of CTAB-coated GNR suspension and mixed overnight. The coated GNR suspension was spun down twice by centrifugation at 10 000 rpm for 10 min and re-suspended in milli-Q water.

Surface modification of GNR with DSPE-PEG-SH suspended in water (DSPE-PEG-GNR/water). A volume of 1.0 mL of aqueous solution of DSPE-PEG-SH (20 mg/mL) was transferred to 10.0 mL of CTAB-coated GNR suspension and mixed overnight. The coated GNR suspension was spun down twice by centrifugation at 10 000 rpm for 10 min and re-suspended in milli-Q water.

Surface modification of GNR with DSPE-PEG-SH suspended in toluene (DSPE-PEG-GNR/toluene). DSPE-PEG-GNR suspended in toluene were prepared by ligand exchange method[34]. The thiolated DSPE-PEG polymer was transferred from water to dichloromethane (DCM) and the dried DSPE-PEG-GNR were suspended in toluene using sonication for 20 min.

Surface modification of GNR with Chol-PEG-SH (Chol-PEG-GNR). A volume of 1.0 mL of aqueous solution of Chol-PEG-SH (20 mg/mL) was transferred to 10 mL of CTAB-coated GNR suspension and mixed overnight. The coated GNR suspension was spun down twice by centrifugation at 10 000 rpm for 10 min and suspended in milli-Q water.

^{1}H NMR analysis of CTAB-GNR, DSPE-PEG-GNR and Chol-PEG-GNR. Samples were dissolved in $CDCl_3$ using a Shigemi NMR microtube. Sodium trimethylsilyl-[2,2,3,3-d4]-propionate (TSP) was employed as an internal standard. An acquisition time of 3.11 s, a relaxation delay of 6 s and 128 transients of a spectral width of 8333.3 Hz were recorded into 65 k time domain points.

Characterization of GNR coated with PEG-SH-containing different functionalities. The synthesized GNR suspensions were characterized by optical absorption spectroscopy, DLS, effective surface charge, TEM and ^{1}H-NMR.

Preparation of human skin samples. Human skin samples were received from a healthy female aged 32 years after undergoing an abdominal plastic surgery. Informed consent was obtained from the donor for study participation and the experimental protocols were approved by Al-Zaytoonah University of Jordan Research Ethics Committee (ZUJ-RES 2018/64/04) in adherence to Helsinki Guidelines.

The obtained skin was cleaned from the subcutaneous fat and stored at −80 °C till use[34].

The colloidal stability of GNR of different surface functionalities upon contact with human skin surface. A volume of 400 µL (4.0 nM) of the following GNR suspensions: m-PEG-GNR, COOH-PEG-GNR, NH_2-PEG-GNR, DSPE-PEG-GNR, and Chol-PEG-GNR were placed into the donor chambers of FDCs. Normal saline (pH ~7.4) was added to the receiver chambers and the FDCs were incubated at 37 °C for 24 hr.

Samples of the applied GNR were taken after 24 hr of skin exposure, and their colloidal stability was evaluated by inspecting their colloidal color, UV-vis absorption spectra, hydrodynamic size and effective surface charge.

Skin permeation study of GNR of different particle sizes and surface functionalities. A volume of 400 µL (4.0 nM) of the following GNR suspensions: m-PEG-GNR (AR ~ 4), m-PEG-GNR (AR ~ 2), COOH-PEG-GNR, NH_2-PEG-GNR, DSPE-PEG-GNR/water, DSPE-PEG-GNR/toluene, and Chol-PEG-GNR were placed into the donor chambers of FDCs. Normal saline (pH ~7.4) was added to the receiver chambers and the FDCs were incubated at 37 °C for 24 hr.

Determination of gold quantities accumulated into skin layers using ICP-OES. After 24 hr incubation, the treated skin samples described in the previous section were prepared for gold analysis by ICP-OES as described previously[34]. Briefly, for each skin sample, the treated skin surface was swabbed using medical cotton to remove the excess amount of GNR. After that, SC layers were collected and separated from the dermis layer by the tape stripping technique using 20 adhesive tapes. The collected skin layers were lysed with 2.0 mL aqua regia (1HNO_3:3HCL), diluted with milli-Q water, filtered using 0.22 µm filters and their gold content was measured by ICE-OES.

The analysis conditions were optimized as described previously[34]. Gold ions were measured at 242.795 nm and the gold concentration (mg/L) was estimated using a standard calibration curve of gold standard for ICP (0.1–10.0 ppm). The results presented as mean ± SD from at least three independent experiments.

Imaging of skin samples pre-treated with GNR of different surface functionalities using confocal laser scanning microscopy. Cleaned human skin samples were incubated for 24 hr with 400 µL (4.0 nM) of DSPE-PEG-GNR, Chol-PEG-GNR, m-PEG-GNR, NH_2-PEG-GNR, COOH-PEG-GNR or milli-Q water (as a control) using FDCs. The skin samples were processed and fixed as thin slices (5 µm) on slides for confocal fluorescence imaging as described previously[38]. The optical excitation and emission wavelengths were 514 and 532 nm, respectively and the image size was around 424.27 µm × 424.27 µm.

The obtained images were analyzed by ImageJ 1.52a software (National Institute of Health, USA), and the fluorescence intensities were estimated as an average fluorescence intensity of at least three images, graphed and provided as charts.

Imaging of skin samples pre-treated with DSPE-PEG-GNR and PEG-GNR by TEM. Skin samples treated with DSPE-PEG-GNR or milli-Q water (as a control) for 24 h were imaged using TEM to evaluate the penetration and accumulation pattern of GNR. The samples were fixed in glutaraldehyde solution (3%) and the fixed tissues were prepared for TEM imaging as described previously[38]. Briefly, tissues were post-fixed in osmium tetraoxide buffer solution and were dehydrated in ethanol solutions, loaded in epoxy resin, sectioned into ~70 nm thin sections, fixed onto the grids and visualized by TEM.

Determination of MIC values of DSPE-PEG-GNR and Chol-PEG-GNR. The MIC values of DSPE-PEG-GNR and Chol-PEG-GNR against *S. aureus* were determined using the two-fold broth microdilution method[71]. A volume of 150 µL of Mueller–Hinton broth was placed in the wells and the GNR suspension (150 µL, 4.0 nM) was added to the first well. Then, serial dilutions (double fold) were performed throughout the plate. A 15 µL of MacFarland adjusted overnight culture of *S. aureus* was added to each well to obtain an average inoculum size of *ca.* 1.0×10^6 CFU/mL. The plates were incubated overnight at 37 °C, and the MIC value was calculated as the average concentration of the well having turbidity and that clear[71]. The previous MIC set up was used to determine the percentage and log reduction in *S. aureus* using the standard plate viable count method at the last well showing no bacterial growth[72]. The antibacterial activity of the coating materials (DSPE-PEG-SH and Chol-PEG-SH; 1.0 mg/mL) was performed using the method described in this section.

Photothermal-based antibacterial activity of DSPE-PEG-GNR and Chol-PEG-GNR. We followed a previous protocol in evaluating the photothermal-based antibacterial activity of DSPE-PEG-GNR and Chol-PEG-GNR against *S. aureus*[35]. Briefly, bacterial inoculated wells (*ca.* 1.0×10^6 CFU/mL) containing DSPE-PEG-GNR at concentrations of 0.004 and 0.002 nM (sub-MIC values), Chol-PEG-GNR at concentrations of 0.125 and 0.06 nM (sub-MIC values) and the negative control (no GNR) were incubated at 37 °C for 10 min and then excited with a laser beam (808 nm, ~3 W/cm^2), at an area of ~0.5 cm^2 for 15 min. The same above set up plate was incubated in dark condition without laser for 25 min at 37 °C. The percentage and log reduction in *S. aureus* viable count at the sub-MIC values were estimated using the standard plate viable count method[72].

Imaging of S. aureus pre-treated with DSPE-PEG-GNR and Chol-PEG-GNR by TEM. A mixture of an overnight cultured *S. aureus* (1.0 mL, 1.0×10^6 CFU/mL) and DSPE-PEG-GNR or Chol-PEG-GNR (200 µL, 4.0 nM) was incubated for 4 hr. Then, the mixture was spun down and the bacterial pellets were fixed in 3% glutaraldehyde and processed as described previously[35]. Sections of 70 nm thickness were obtained and fixed onto Formvar copper grids and imaged by TEM. Untreated bacteria fixed as previously described was used as a control.

Statistical analysis. Unpaired t-test was employed for statistical analysis employing GraphPad Prism, version 7.0. When $p < 0.05$, the results are considered significant.

Data Availability

The datasets generated and/or analyzed during the current study are available from the corresponding author on reasonable request.

References

1. Kurmi, B. D., Tekchandani, P., Paliwal, R. & Paliwal, S. R. Transdermal Drug Delivery: Opportunities and Challenges for Controlled Delivery of Therapeutic Agents Using Nanocarriers. *Current drug metabolism* **18**, 481–495, https://doi.org/10.2174/1389200218666170222150555 (2017).
2. Carazo, E. *et al*. Advanced Inorganic Nanosystems for Skin Drug Delivery. *The Chemical Record* **18**, 891–899, https://doi.org/10.1002/tcr.201700061 (2018).
3. Elias, P. M. Epidermal lipids, barrier function, and desquamation. *The Journal of investigative dermatology* **80**(Suppl), 44s–49s (1983).
4. Williams, M. L. & Elias, P. M. From basket weave to barrier. Unifying concepts for the pathogenesis of the disorders of cornification. *Archives of dermatology* **129**, 626–629 (1993).
5. van Smeden, J. & Bouwstra, J. A. Stratum Corneum Lipids: Their Role for the Skin Barrier Function in Healthy Subjects and Atopic Dermatitis Patients. *Current problems in dermatology* **49**, 8–26, https://doi.org/10.1159/000441540 (2016).
6. Szunerits, S. & Boukherroub, R. Heat: A Highly Efficient Skin Enhancer for Transdermal Drug Delivery. *Frontiers in bioengineering and biotechnology* **6**, 15, https://doi.org/10.3389/fbioe.2018.00015 (2018).
7. Amjadi, M., Mostaghaci, B. & Sitti, M. Recent Advances in Skin Penetration Enhancers for Transdermal Gene and Drug Delivery. *Current gene therapy* **17**, 139–146, https://doi.org/10.2174/1566523217666170510151540 (2017).
8. Dave, K. & Krishna Venuganti, V. V. Dendritic polymers for dermal drug delivery. *Therapeutic delivery* **8**, 1077–1096, https://doi.org/10.4155/tde-2017-0091 (2017).
9. Md, S. *et al*. Lipid based nanocarriers system for topical delivery of photosensitizers. *Drug discovery today* **22**, 1274–1283, https://doi.org/10.1016/j.drudis.2017.04.010 (2017).
10. Niska, K., Zielinska, E., Radomski, M. W. & Inkielewicz-Stepniak, I. Metal nanoparticles in dermatology and cosmetology: Interactions with human skin cells. *Chemico-biological interactions* **295**, 38–51, https://doi.org/10.1016/j.cbi.2017.06.018 (2018).
11. Hussain, A. *et al*. Elastic liposomes as novel carriers: recent advances in drug delivery. *International journal of nanomedicine* **12**, 5087–5108, https://doi.org/10.2147/ijn.S138267 (2017).
12. Tiwari, P. M., Vig, K., Dennis, V. A. & Singh, S. R. Functionalized Gold Nanoparticles and Their Biomedical Applications. *Nanomaterials (Basel, Switzerland)* **1**, 31–63, https://doi.org/10.3390/nano1010031 (2011).
13. Choi, W. I., Sahu, A., Kim, Y. H. & Tae, G. Photothermal cancer therapy and imaging based on gold nanorods. *Annals of biomedical engineering* **40**, 534–546, https://doi.org/10.1007/s10439-011-0388-0 (2012).
14. Alkilany, A. M., Lohse, S. E. & Murphy, C. J. The gold standard: gold nanoparticle libraries to understand the nano-bio interface. *Accounts of chemical research* **46**, 650–661, https://doi.org/10.1021/ar300015b (2013).
15. Huang, X., Jain, P. K., El-Sayed, I. H. & El-Sayed, M. A. Plasmonic photothermal therapy (PPTT) using gold nanoparticles. *Lasers in medical science* **23**, 217–228, https://doi.org/10.1007/s10103-007-0470-x (2008).
16. Schneider, M., Stracke, F., Hansen, S. & Schaefer, U. F. Nanoparticles and their interactions with the dermal barrier. *Dermato-endocrinology* **1**, 197–206 (2009).
17. Sonavane, G. *et al*. *In vitro* permeation of gold nanoparticles through rat skin and rat intestine: effect of particle size. *Colloids and surfaces. B, Biointerfaces* **65**, 1–10, https://doi.org/10.1016/j.colsurfb.2008.02.013 (2008).
18. Fernandes, R. *et al*. Interactions of skin with gold nanoparticles of different surface charge, shape, and functionality. *Small (Weinheim an der Bergstrasse, Germany)* **11**, 713–721, https://doi.org/10.1002/smll.201401913 (2015).
19. Lee, O. *et al*. Influence of surface charge of gold nanorods on skin penetration. *Skin research and technology: official journal of International Society for Bioengineering and the Skin (ISBS) [and] International Society for Digital Imaging of Skin (ISDIS) [and] International Society for Skin Imaging (ISSI)* **19**, e390–396, https://doi.org/10.1111/j.1600-0846.2012.00656.x (2013).
20. Kang, J. H. & Ko, Y. T. Lipid-coated gold nanocomposites for enhanced cancer therapy. *International journal of nanomedicine* **10**(Spec Iss), 33–45, https://doi.org/10.2147/ijn.S88307 (2015).
21. Woo, J. O., Misran, M., Lee, P. F. & Tan, L. P. Development of a controlled release of salicylic acid loaded stearic acid-oleic acid nanoparticles in cream for topical delivery. *TheScientificWorldJournal* **2014**, 205703, https://doi.org/10.1155/2014/205703 (2014).
22. Kumar, A. *et al*. Permeation of antigen protein-conjugated nanoparticles and live bacteria through microneedle-treated mouse skin. *International journal of nanomedicine* **6**, 1253–1264, https://doi.org/10.2147/ijn.S20413 (2011).
23. Jin, S. E. & Kim, C. K. Charge-mediated topical delivery of plasmid DNA with cationic lipid nanoparticles to the skin. *Colloids and surfaces. B, Biointerfaces* **116**, 582–590, https://doi.org/10.1016/j.colsurfb.2014.01.053 (2014).
24. Li, L. L. *et al*. Biomimetic surface engineering of lanthanide-doped upconversion nanoparticles as versatile bioprobes. *Angewandte Chemie (International ed. in English)* **51**, 6121–6125, https://doi.org/10.1002/anie.201109156 (2012).
25. Zheng, W. *et al*. Quantum dots encapsulated within phospholipid membranes: phase-dependent structure, photostability, and site-selective functionalization. *Journal of the American Chemical Society* **136**, 1992–1999, https://doi.org/10.1021/ja411339f (2014).
26. Yang, C. T. *et al*. Room-temperature copper-catalyzed carbon-nitrogen coupling of aryl iodides and bromides promoted by organic ionic bases. *Angewandte Chemie (International ed. in English)* **48**, 7398–7401, https://doi.org/10.1002/anie.200903158 (2009).
27. Wang, L. S. *et al*. Biofunctionalized phospholipid-capped mesoporous silica nanoshuttles for targeted drug delivery: improved water suspensibility and decreased nonspecific protein binding. *ACS Nano* **4**, 4371–4379, https://doi.org/10.1021/nn901376h (2010).
28. Tao, Y., Li, M., Kim, B. & Auguste, D. T. Incorporating gold nanoclusters and target-directed liposomes as a synergistic amplified colorimetric sensor for HER2-positive breast cancer cell detection. *Theranostics* **7**, 899–911, https://doi.org/10.7150/thno.17927 (2017).
29. Wang, M. & Petersen, N. O. Lipid-coated gold nanoparticles promote lamellar body formation in A549 cells. *Biochimica et biophysica acta* **1831**, 1089–1097, https://doi.org/10.1016/j.bbalip.2013.01.018 (2013).
30. Wen, Q., Liu, S. J., Tang, L. J., Tang, Y. & Jiang, J. H. Gold nanoparticle supported phospholipid membranes as a biomimetic biosensor platform for phosphoinositide signaling detection. *Biosensors & bioelectronics* **62**, 113–119, https://doi.org/10.1016/j.bios.2014.06.016 (2014).
31. Lee, S. E. *et al*. Biologically functional cationic phospholipid-gold nanoplasmonic carriers of RNA. *Journal of the American Chemical Society* **131**, 14066–14074, https://doi.org/10.1021/ja904326j (2009).
32. Hu, X., Yang, F., Liao, Y., Li, L. & Zhang, L. Cholesterol-PEG comodified poly (N-butyl) cyanoacrylate nanoparticles for brain delivery: *in vitro* and *in vivo* evaluations. *Drug Deliv* **24**, 121–132, https://doi.org/10.1080/10717544.2016.1233590 (2017).
33. Baroli, B. Penetration of nanoparticles and nanomaterials in the skin: fiction or reality? *Journal of pharmaceutical sciences* **99**, 21–50, https://doi.org/10.1002/jps.21817 (2010).
34. Mahmoud, N. N. *et al*. Preferential accumulation of gold nanorods into human skin hair follicles: Effect of nanoparticle surface chemistry. *Journal of Colloid and Interface Science* **503**, 95–102, https://doi.org/10.1016/j.jcis.2017.05.011 (2017).
35. Mahmoud, N. N., Alkilany, A. M., Khalil, E. A. & Al-Bakri, A. G. Nano-Photothermal ablation effect of Hydrophilic and Hydrophobic Functionalized Gold Nanorods on Staphylococcus aureus and Propionibacterium acnes. *Sci Rep* **8**, 6881, https://doi.org/10.1038/s41598-018-24837-7 (2018).

36. Norman, R. S., Stone, J. W., Gole, A., Murphy, C. J. & Sabo-Attwood, T. L. Targeted photothermal lysis of the pathogenic bacteria, Pseudomonas aeruginosa, with gold nanorods. *Nano Lett* **8**, 302–306, https://doi.org/10.1021/nl0727056 (2008).
37. Mahmoud, N. N., Alkilany, A. M., Khalil, E. A. & Al-Bakri, A. G. Antibacterial activity of gold nanorods against Staphylococcus aureus and Propionibacterium acnes: misinterpretations and artifacts. *International journal of nanomedicine* **12**, 7311–7322, https://doi.org/10.2147/ijn.S145531 (2017).
38. Mahmoud, N. N. *et al*. Synchrotron-based X-ray fluorescence study of gold nanorods and skin elements distribution into excised human skin layers. *Colloids and surfaces. B, Biointerfaces* **165**, 118–126, https://doi.org/10.1016/j.colsurfb.2018.02.021 (2018).
39. Nakata, K., Tsuchido, T. & Matsumura, Y. Antimicrobial cationic surfactant, cetyltrimethylammonium bromide, induces superoxide stress in Escherichia coli cells. *Journal of applied microbiology* **110**, 568–579, https://doi.org/10.1111/j.1365-2672.2010.04912.x (2011).
40. Hinterwirth, H. *et al*. Quantifying Thiol Ligand Density of Self-Assembled Monolayers on Gold Nanoparticles by Inductively Coupled Plasma–Mass Spectrometry. *ACS Nano* **7**, 1129–1136, https://doi.org/10.1021/nn306024a (2013).
41. Gao, J., Huang, X., Liu, H., Zan, F. & Ren, J. Colloidal Stability of Gold Nanoparticles Modified with Thiol Compounds: Bioconjugation and Application in Cancer Cell Imaging. *Langmuir: the ACS journal of surfaces and colloids* **28**, 4464–4471, https://doi.org/10.1021/la204289k (2012).
42. Mahmoud, N. N., Al-Qaoud, K. M., Al-Bakri, A. G., Alkilany, A. M. & Khalil, E. A. Colloidal stability of gold nanorod solution upon exposure to excised human skin: Effect of surface chemistry and protein adsorption. *The international journal of biochemistry & cell biology* **75**, 223–231, https://doi.org/10.1016/j.biocel.2016.02.020 (2016).
43. Guo, C. & Yarger, J. L. Characterizing gold nanoparticles by NMR spectroscopy. *Magnetic Resonance in Chemistry* **56**, 1074–1082, https://doi.org/10.1002/mrc.4753 (2018).
44. Schuetze, B. *et al*. Conjugation of thiol-terminated molecules to ultrasmall 2 nm-gold nanoparticles leads to remarkably complex 1H-NMR spectra. *Journal of Materials Chemistry B* **4**, 2179–2189, https://doi.org/10.1039/C5TB02443A (2016).
45. Orendorff, C. J., Alam, T. M., Sasaki, D. Y., Bunker, B. C. & Voigt, J. A. Phospholipid-gold nanorod composites. *ACS Nano* **3**, 971–983, https://doi.org/10.1021/nn900037k (2009).
46. Fulmer, G. R. *et al*. NMR Chemical Shifts of Trace Impurities: Common Laboratory Solvents, Organics, and Gases in Deuterated Solvents Relevant to the Organometallic Chemist. *Organometallics* **29**, 2176–2179, https://doi.org/10.1021/om100106e (2010).
47. Karakoti, A. S., Das, S., Thevuthasan, S. & Seal, S. PEGylated inorganic nanoparticles. *Angewandte Chemie (International ed. in English)* **50**, 1980–1994, https://doi.org/10.1002/anie.201002969 (2011).
48. D'Souza, A. A. & Shegokar, R. Polyethylene glycol (PEG): a versatile polymer for pharmaceutical applications. *Expert opinion on drug delivery* **13**, 1257–1275, https://doi.org/10.1080/17425247.2016.1182485 (2016).
49. Alkilany, A. M. *et al*. Cellular uptake and cytotoxicity of gold nanorods: molecular origin of cytotoxicity and surface effects. *Small (Weinheim an der Bergstrasse, Germany)* **5**, 701–708, https://doi.org/10.1002/smll.200801546 (2009).
50. Potts, R. Skin Barrier: Principles of Percutaneous Absorption. *Archives of dermatology* **133**, 924–924, https://doi.org/10.1001/archderm.1997.03890430146031 (1997).
51. Labouta, H. I., el-Khordagui, L. K., Kraus, T. & Schneider, M. Mechanism and determinants of nanoparticle penetration through human skin. *Nanoscale* **3**, 4989–4999, https://doi.org/10.1039/c1nr11109d (2011).
52. Zhang, L. W. & Monteiro-Riviere, N. A. Use of confocal microscopy for nanoparticle drug delivery through skin. *Journal of biomedical optics* **18**, 061214, https://doi.org/10.1117/1.Jbo.18.6.061214 (2013).
53. Leite-Silva, V. R. *et al*. Human skin penetration and local effects of topical nano zinc oxide after occlusion and barrier impairment. *European journal of pharmaceutics and biopharmaceutics: official journal of Arbeitsgemeinschaft fur Pharmazeutische Verfahrenstechnik e.V* **104**, 140–147, https://doi.org/10.1016/j.ejpb.2016.04.022 (2016).
54. Kocbek, P., Teskac, K., Kreft, M. E. & Kristl, J. Toxicological aspects of long-term treatment of keratinocytes with ZnO and TiO2 nanoparticles. *Small (Weinheim an der Bergstrasse, Germany)* **6**, 1908–1917, https://doi.org/10.1002/smll.201000032 (2010).
55. Pawar, K. R. & Babu, R. J. Lipid materials for topical and transdermal delivery of nanoemulsions. *Critical reviews in therapeutic drug carrier systems* **31**, 429–458 (2014).
56. Salim, N. *et al*. Nanoemulsion as a topical delivery system of antipsoriatic drugs. *RSC Advances* **6**, 6234–6250, https://doi.org/10.1039/C5RA14946K (2016).
57. Garces, A., Amaral, M. H., Sousa Lobo, J. M. & Silva, A. C. Formulations based on solid lipid nanoparticles (SLN) and nanostructured lipid carriers (NLC) for cutaneous use: A review. *European journal of pharmaceutical sciences: official journal of the European Federation for Pharmaceutical Sciences* **112**, 159–167, https://doi.org/10.1016/j.ejps.2017.11.023 (2018).
58. Roberts, M. S. *et al*. Topical and cutaneous delivery using nanosystems. *Journal of controlled release: official journal of the Controlled Release Society* **247**, 86–105, https://doi.org/10.1016/j.jconrel.2016.12.022 (2017).
59. Prow, T. W. *et al*. Quantum dot penetration into viable human skin. *Nanotoxicology* **6**, 173–185, https://doi.org/10.3109/17435390.2011.569092 (2012).
60. Zhang, W. *et al*. Penetration and distribution of PLGA nanoparticles in the human skin treated with microneedles. *International journal of pharmaceutics* **402**, 205–212, https://doi.org/10.1016/j.ijpharm.2010.09.037 (2010).
61. Akbarzadeh, A. *et al*. Liposome: classification, preparation, and applications. *Nanoscale research letters* **8**, 102, https://doi.org/10.1186/1556-276x-8-102 (2013).
62. Dreaden, E. C., Austin, L. A., Mackey, M. A. & El-Sayed, M. A. Size matters: gold nanoparticles in targeted cancer drug delivery. *Therapeutic delivery* **3**, 457–478 (2012).
63. Zellmer, S., Pfeil, W. & Lasch, J. Interaction of phosphatidylcholine liposomes with the human stratum corneum. *Biochimica et Biophysica Acta (BBA) - Biomembranes* **1237**, 176–182, https://doi.org/10.1016/0005-2736(95)00100-H (1995).
64. Kirjavainen, M. *et al*. Interaction of liposomes with human skin *in vitro* — The influence of lipid composition and structure. *Biochimica et Biophysica Acta (BBA) - Lipids and Lipid Metabolism* **1304**, 179–189, https://doi.org/10.1016/S0005-2760(96)00126-9 (1996).
65. Kirjavainen, M. *et al*. Phospholipids affect stratum corneum lipid bilayer fluidity and drug partitioning into the bilayers. *Journal of controlled release: official journal of the Controlled Release Society* **58**, 207–214 (1999).
66. Iannuccelli, V. *et al*. *In vivo* penetration of bare and lipid-coated silica nanoparticles across the human stratum corneum. *Colloids and surfaces. B, Biointerfaces* **122**, 653–661, https://doi.org/10.1016/j.colsurfb.2014.07.046 (2014).
67. Dumontel, B. *et al*. Enhanced biostability and cellular uptake of zinc oxide nanocrystals shielded with a phospholipid bilayer. *Journal of Materials Chemistry B* **5**, 8799–8813, https://doi.org/10.1039/C7TB02229H (2017).
68. Israelachvili, J. The different faces of poly(ethylene glycol). *Proceedings of the National Academy of Sciences of the United States of America* **94**, 8378–8379 (1997).
69. Gupta, R. & Rai, B. Effect of Size and Surface Charge of Gold Nanoparticles on their Skin Permeability: A Molecular Dynamics Study. *Sci Rep* **7**, 45292, https://doi.org/10.1038/srep45292 (2017).
70. Tong, S. Y., Davis, J. S., Eichenberger, E., Holland, T. L. & Fowler, V. G. Jr. Staphylococcus aureus infections: epidemiology, pathophysiology, clinical manifestations, and management. *Clinical microbiology reviews* **28**, 603–661, https://doi.org/10.1128/cmr.00134-14 (2015).
71. The Clinical and Laboratory Standards Institute for antimicrobial susceptibility testing (CLSI). (Wayne, 2016).
72. M26-A. Methods for Determining Bactericidal Activity of Antimicrobial Agents; Approved Guideline. (PA: USA; 1999).

73. Taheri, S. *et al*. Antibacterial Plasma Polymer Films Conjugated with Phospholipid Encapsulated Silver Nanoparticles. *ACS Biomaterials Science & Engineering* **1**, 1278–1286, https://doi.org/10.1021/acsbiomaterials.5b00338 (2015).
74. Millenbaugh, N. J., Baskin, J. B., DeSilva, M. N., Elliott, W. R. & Glickman, R. D. Photothermal killing of Staphylococcus aureus using antibody-targeted gold nanoparticles. *International journal of nanomedicine* **10**, 1953–1960, https://doi.org/10.2147/ijn.S76150 (2015).

Acknowledgements

This work was funded by Abdul Hameed Shoman Foundation (AHSF), Amman, Jordan, Grant 3/2017, and Al-Zaytoonah University of Jordan (Deanship of Scientific Research and Graduate Studies), Grant 2017-2016/64/04.

Author Contributions

N.N.M. designed the research; N.N.M., J.A.A., A.A.A., A.G.A., R.H., and E.A.K. conducted the experiments. All authors contributed in analyzing the results and writing the article.

Additional Information

Supplementary information accompanies this paper at https://doi.org/10.1038/s41598-019-42047-7.

Competing Interests: The authors declare no competing interests.

Publisher's note: Springer Nature remains neutral with regard to jurisdictional claims in published maps and institutional affiliations.

Open Access This article is licensed under a Creative Commons Attribution 4.0 International License, which permits use, sharing, adaptation, distribution and reproduction in any medium or format, as long as you give appropriate credit to the original author(s) and the source, provide a link to the Creative Commons license, and indicate if changes were made. The images or other third party material in this article are included in the article's Creative Commons license, unless indicated otherwise in a credit line to the material. If material is not included in the article's Creative Commons license and your intended use is not permitted by statutory regulation or exceeds the permitted use, you will need to obtain permission directly from the copyright holder. To view a copy of this license, visit http://creativecommons.org/licenses/by/4.0/.

© The Author(s) 2019